

Nanoscale

Accepted Manuscript



This is an *Accepted Manuscript*, which has been through the Royal Society of Chemistry peer review process and has been accepted for publication.

Accepted Manuscripts are published online shortly after acceptance, before technical editing, formatting and proof reading. Using this free service, authors can make their results available to the community, in citable form, before we publish the edited article. We will replace this *Accepted Manuscript* with the edited and formatted *Advance Article* as soon as it is available.

You can find more information about *Accepted Manuscripts* in the [Information for Authors](#).

Please note that technical editing may introduce minor changes to the text and/or graphics, which may alter content. The journal's standard [Terms & Conditions](#) and the [Ethical guidelines](#) still apply. In no event shall the Royal Society of Chemistry be held responsible for any errors or omissions in this *Accepted Manuscript* or any consequences arising from the use of any information it contains.



Smart nanogels at the at the air/water interface: structural studies by neutron reflectivity

Katarzyna Zielińska,^a Huihui Sun,^a Richard A. Campbell,^b Ali Zarbakhsh^{a*} and Marina Resmini^{a*}

Received 00th January 20xx,
Accepted 00th January 20xx

DOI: 10.1039/x0xx00000x

www.rsc.org/

The development of effective transdermal drug delivery systems based on nanosized polymers requires a better understanding of the behaviour of such nanomaterials at interfaces. *N*-isopropylacrylamide-based nanogels synthesized with different percentages of *N,N'*-methylenebisacrylamide as cross-linker, ranging from 10 to 30%, were characterized at physiological temperature at the air/water interface, using neutron reflectivity (NR), with isotopic contrast variation, and surface tension measurements; this allowed us to resolve the adsorbed amount and the volume fraction of nanogels at the interface. A large conformational change for the nanogels results in strong deformations at the interface. As the percentage of cross-linker incorporated in the nanogels becomes higher, more rigid matrices are obtained, although less deformed, and the amount of adsorbed nanogels is increased. The data provide the first experimental evidence of structural changes of nanogels as a function of the degree of cross-linking at the air/water interface.

Introduction

The past decade has seen nanomaterials receive increasing attention in theoretical studies on soft matter and in applied fields¹, especially in biomedical applications². Organic polymeric nanoparticles have attracted great interest, due to the possibility of tailoring their chemical structure and physico- and chemical properties to specific applications. Among the different polymeric nanoparticles that have been investigated^{3,4}, nanogels offer attractive features. They are covalently cross-linked polymers, characterized by small size, high surface-to-volume ratio and the ability to create stable colloidal solutions in the appropriate solvent system^{5,6}, combining properties of typical colloids with the soft character and responsiveness of gels⁷. Of particular interest has been the development of such gels that exhibit a phase transition in response to changes in temperature, pH, ionic strength and light, among others, and which are frequently reported in the literature as “switchable” or “smart” materials^{8,9}. The choice of stimuli depends on the application, with temperature being one of the most frequently investigated¹⁰.

N-isopropylacrylamide (NIPAM) is a monomer that has been extensively studied and used for the development of a large number of polymeric matrices that display thermoresponsiveness¹¹ at different temperatures, depending on the chemical structure of

the system. In its linear form poly(*N*-isopropylacrylamide) (PNIPAM) has a lower critical solution temperature (LCST) around 32°C, which can be significantly tailored to higher and lower values by the addition of comonomers and cross-linkers. In addition to their ability to adjust conformation with temperature, NIPAM-based polymers can adsorb at interfaces (fluid/solid and fluid/fluid) and be surface active (i.e. lower the surface tension of water)¹². Given the importance of fluid interfaces both in nature and industry, surface active materials are intensively studied for a number of applications, ranging from nanomedicine and drug delivery to fine chemistry and the oil industry¹³.

The development and use of NIPAM-based nanogels to stabilize interfaces has already been reported^{14,15}, although the stabilization and destabilization mechanisms involved using such matrices are still the object of fierce debate^{12,16,17}. An understanding of how these particles stabilize a given interface and the resolution of their conformations at the surface are important issues that would help the optimization of the use of these nanoparticles in specific applications. Despite a number of studies on adsorbed NIPAM-based microgels reported in the literature^{18,19}, the process of controlling adsorption is still not well understood. There also exists a dearth of experimental data on the adsorption dynamics of these particles at fluid interfaces. Thus the investigation of the behaviour of nanogels at interfaces is of great importance.

To date, most of the studies on the interfacial properties of thermo-sensitive polymers focussed on linear PNIPAM^{17,20}. A few of the existing works on the interfacial behaviour of NIPAM microgels are based on surface tension measurements^{19,21}, particle-tracking and surface compression rheology²². These studies have given useful information on kinetics and general insight into the adsorption process of gel particles, although information concerning the structure of the adsorbed layer was not obtained. To get more direct and detailed data on nanoparticles behaviour at interfaces

^a Department of Chemistry, SBCS, Queen Mary University of London, Mile End Road, London E1 4NS, United Kingdom, e-mails: a.zarbakhsh@qmul.ac.uk, m.resmini@qmul.ac.uk

^b Institut Laue-Langevin, 71 avenue des Martyrs - CS 20156, 38042 Grenoble Cedex 9, France

† Footnotes relating to the title and/or authors should appear here.

Electronic Supplementary Information (ESI) available: [details of any supplementary information available should be included here]. See DOI: 10.1039/x0xx00000x

neutron reflectivity (NR) has proved to be a sensitive technique. Recently NR was successfully used to determine contact angle and adsorption energies of nanoparticles at air-liquid interface²³. Furthermore NR studies of linear PNIPAM at air/water interfaces has revealed that the polymer forms a thin layer (~1.5 nm) with low water content in contact with air at temperatures below the LCST²⁴. A more dilute layer extending toward the bulk solution with a thickness of up to the radius of gyration of the polymer is located next to this near-surface layer²⁵.

Continuing our work on the synthesis of polymeric organic nanogels and their characterization^{5,26} supported by NR studies²⁷, we developed an interest in the use of such nanogels as delivery systems targeting the skin. The large surface area of the skin offers a non-invasive, patient friendly administration route to the blood system that helps to avoid first pass metabolism and maintain steady plasma concentration of the drug. Despite considerable efforts, results to date on materials that can effectively cross the *Stratum Corneum* of the skin are not satisfactory for clinical purposes. It is crucially important to understand the behaviour of nanoparticles at the interface to design novel delivery systems with improved skin penetration efficiency. Hence studying these systems at the air-water interface would be the first step in that direction. We present here our recent findings on the synthesis and characterization of *N*-isopropylacrylamide nanogels crosslinked with *N,N'*-methylenebisacrylamide (MBA) and on the evaluation of their behaviour at the air/water interface. We explore the impact of the nanogel morphology (determined by the amount of cross-linker) on the adsorption kinetics and adsorbed amount at physiological temperature. We report also an in-depth study of the structure of the adsorbed nanogel layer at the air/water interface and correlate it with the nanogel surface activity.

Materials and methods

Materials

N-isopropylacrylamide (NIPAM, 97%), *N,N'*-methylenebisacrylamide (MBA, 99%) and D₂O were purchased from Sigma Aldrich and used as provided. 2,2'-Azobis(2-methylpropionitrile) (AIBN, 98%, Sigma Aldrich) was recrystallized from methanol. Anhydrous dimethyl sulfoxide (DMSO, 99.8%) was purchased from Alfa Aesar. Deuterated *N*-isopropylacrylamide with seven deuterium atoms in the isopropyl groups (NIPAM D7) was obtained from Polymer Source (Canada). Dialysis membrane (MWCO 3500 Da) was purchased from Medicell International Ltd. The ultrapure deionized water was prepared by the Purelab option water purification system (Elga).

Nanogel synthesis

Nanogels were obtained with the following standard procedure previously reported⁵. NIPAM and MBA in different ratios (see Table 1) were dissolved in the required volume of DMSO, as solvent, to give $C_M = 1\%$ (C_M represents the critical monomer concentration, at which micro-gelation rather than macro-gelation occurs). AIBN was added to the solution in a Wheaton bottle, which was sealed, degassed and flushed with nitrogen at least five times. The reaction was initiated by placing the bottle at 70°C for 24 hours.

Table 1. The composition and polymerization yield (Y) of NIPAM and NIPAM D7 based nanogels

sample	% mol monomer	% mol MBA	Y, %
10 MBA	90	10	72
20 MBA	80	20	66
30 MBA	70	30	69
50 MBA	50	50	60
10 MBA D7	90	10	77
20 MBA D7	80	20	65
30 MBA D7	70	30	70
50 MBA D7	50	50	52

MBA – *N,N'*-methylenebisacrylamide, Y – polymerization yield

The clear solution was dialyzed (MWCO 3500 Da) against deionized water for 3 days with frequent changes, followed by freeze-drying (Labconco freeZone 6) to give white flakes. Deuterated nanogels were synthesized following the same procedure, but using NIPAM D7 as monomer.

Dispersions of nanogels were prepared by weighing the desired amount of material in the required solvent, followed by sonication of the solution for 2 minutes at room temperature. For comparison purposes linear polymers (0% MBA) were prepared as well. Nanogel solutions are prepared by weight as opposed to molar concentration given the uncertainty in determining the molecular weight.

Nanogel characterization

Dynamic light scattering (DLS) measurements of the nanogel radius were performed with a Zetasizer Nano ZS from Malvern Instruments. Measurements were carried out in triplicate on freshly prepared dispersions (concentrations of 1.0 mg ml⁻¹) filtered through a 0.2 μm syringe filter. These nanogels have the potential for biomedical applications; hence measurements were carried out close to physiological temperature (309 K).

The density of the dry nanogels, ρ , was estimated by volume by means of an AccuPyc 1330 helium pycnometer (Micrometrics). The samples were weighed on an analytical balance, and their volume was obtained from the difference of the helium pressure inside the empty chamber and chamber filled with the sample.

The structure of the nanogels was characterized by atomic force microscopy (AFM) and transmission electron microscopy (TEM). For the imaging, the gel particles were deposited on a support (polysine coated microscopy slides, for AFM or on a copper grid for TEM) and dried overnight. AFM imaging was carried out using the ultra-low-amplitude tapping mode on a Veeco Dimension 3100 AFM with the scanning speed of 0.5 Hz and a low-resonance-frequency pyramidal silicon cantilever resonating at 300 kHz (force constant: 40 N/m). The TEM images were obtained using a JEOL JEM-1230 microscope and the samples were viewed at an accelerating voltage of 80 kV.

The surface tension measurements were performed using a Krüss K9S (C11227) Wilhelmy plate tensiometer at 309.0 ± 0.1 K. Freshly prepared nanogel suspensions equilibrated at 309 K (concentration of 5 × 10⁻³ mg ml⁻¹) were poured carefully into the thermostated tensiometer trough. The surface tension values were then recorded as a function of time at 1 minute intervals.

The optical transmittance of nanogels (concentration of 1.0 mg ml⁻¹) in deionized water was measured at 500 nm at temperatures

ranging from 20°C to 65°C with a Cary 100 UV-vis spectrophotometer (Ailent Technologies) to estimate the volume phase transition temperature (VPTT) of the specimens. The temperature of the sample solution was adjusted by a temperature controller (Carry). The optical path length of the sample was 10 mm.

Neutron reflectivity, NR

The neutron reflectivity measurements were carried out using the FIGARO reflectometer at the Institut Laue-Langevin (ILL), Grenoble, France²⁸. The reflectivity $R(Q_z)$ was measured using the time-of-flight technique as a function of momentum transfer normal to the interface $Q_z = (4\pi \sin \theta)/\lambda$, where θ is the grazing angle of incidence of neutrons with wavelength λ . The neutron reflectivity profiles were measured at incident angles of $\theta = 0.624^\circ$ and 3.78° ($\lambda = 2\text{--}30 \text{ \AA}$) providing a wide Q_z range. The sample was under-illuminated with a constant resolution $\delta Q/Q \approx 8\%$. All measurements were conducted at $T = 309 \pm 1 \text{ K}$ (below the nanogel transition temperature). The background around the specular reflection peak was subtracted by the use of the 2D detector on FIGARO.

Protonated (NIPAM) and deuterated (NIPAM D7) nanogel dispersions were prepared at a concentration of $5 \times 10^{-3} \text{ mg ml}^{-1}$. D₂O and null reflecting water, NRW (8.1% vol of D₂O in H₂O giving a scattering length density equal to zero) were used as an aqueous sub-phase.

NR data analysis

NR is a technique sensitive to the neutron refractive index profile normal to an interface, $Nb(z)$, averaged over the probed sample region (several cm^2)²⁹. If the sample does not contain strong neutron absorbers (e.g. cadmium or boron), the neutron refractive index can be expressed as:

$$n(\lambda) \approx 1 - \frac{\lambda^2}{2\pi} Nb \quad (1)$$

where N is the atomic number density and b the coherent scattering length. The multiple Nb , referred to as the scattering length density, varies linearly with the volume fraction composition:

$$Nb \approx \sum_i \varphi_i Nb_i \quad (2)$$

where φ_i is the volume fraction and Nb_i the scattering length density of component i , respectively. Possibly the main advantage of neutron reflectivity is that the scattering length b varies with different elements and in particular with different isotopes (e.g. for hydrogen $b_H = -3.74 \text{ fm}$ and deuterium $b_D = 6.67 \text{ fm}$). By changing the isotopic ratio, the Nb of the molecule can be adjusted to match that of other components in the system or to maximize the difference in refractive index. This approach is known as the isotopic contrast variation method.

The data were first normalized and the residual background of 10^{-7} was derived from a least squares fit to an air/D₂O measurement using a capillary wave roughness value of 2.5 \AA . Data were fitted using the optical matrix method³⁰. The interface is represented by models of discrete layers, with each layer having a characteristic thickness (d), composition (Nb) and interlayer roughness (σ) corresponding to regions with different chemical compositions. The

NR data analysis was carried out using two different strategies. In the first step the reflectivity data from the H and D nanogels in NRW recorded at the lower incident angle were analysed in a reduced wavelength range of $4.5\text{--}14 \text{ \AA}$ (Q_z -range of $0.01\text{--}0.03 \text{ \AA}^{-1}$, Fig. S1). In this restricted Q_z -range, the scattering excess of the adsorption layer is highly insensitive to details of the structural model used, hence its analysis results in a precise measure of the adsorbed amount^{31,32}. This model was used to fit the kinetic adsorption data and to obtain the surface excess values, Γ , which are proportional to the product of the fitted scattering length density Nb_{fitted} and thickness of the adsorption layer, d , given by³³:

$$\Gamma = \frac{Nb_{\text{fitted}}d}{\sum bN_A} \quad (3)$$

where N_A is Avogadro's number and b is the mean scattering length of the adsorbed species. For the nanogels, this can then be written as:

$$\Gamma = \varphi_{\text{polymer}} \times \rho \times d \quad (4)$$

where ρ is the physical density of the polymer and φ_{polymer} is the polymer volume fraction calculated from the ratio between the fitted value of Nb_{fitted} and the theoretical scattering length density of the polymer (Nb). A single layer model was used to fit the data solely for the purpose of estimating the surface excess using the program Motofit³⁴. The Nb_{fitted} of the layer was fitted with the a nominal layer thickness of 20 \AA and inter-layer roughnesses of 4 \AA . However given that the adsorbed amount is calculated from the product of the scattering length density and layer thickness, the nominal value chosen for the layer thickness has a minimal influence on the product. To demonstrate this point we have fitted data for 20% MBA sample with different layer thicknesses of 10 \AA , 20 \AA and 40 \AA and the variation in the adsorbed amount is $< 2.4 \%$. In the second step, a more detailed fitting of the data was carried out to ascertain structural information over the full Q_z -range. Data were fitted for a total of four different contrasts (NIPAM protonated and NIPAM D7 nanogels, both in NRW and D₂O as the aqueous sub-phase). A minimum two layer model for the linear polymers and a three layer model for the nanogels were needed to fit all the contrasts consistently. The first layer was composed of solvent, air and polymer. The other one or two layers consisted of polymer and the aqueous sub-phase. The fitted parameters obtained were then used to estimate the volume fractions of polymer (φ_{polymer}) and water (φ_{water}) of the layers.

Results and discussion

The aim of these studies was to contribute to the understanding of the relationship between the percentage of cross-linker in NIPAM-based nanogels and their properties, such as particle size, surface activity and structural conformation at the air/water interface. In order to do this a series of nanogels with varying degree of cross-linker (MBA) were synthesized (details shown in Table 1) by high dilution radical polymerization, a method that does not require the use of surfactants and prevents particle-particle reactivity whilst favouring intramolecular cross-linking. In addition, the use of different total monomer concentrations (C_M) allows a control on the degree of polydispersity and particle size. Nanogel particles were

Table 2. Characterization of NIPAM and NIPAM D7 based nanogels together with calculated values of nanogels scattering length density, Nb

sample	d by AFM, nm	d_h by DLS, nm	Pdl	ρ , $g\text{ ml}^{-1}$	$VPTT$, $^{\circ}\text{C}$	Nb $\times 10^{-6}\text{ \AA}^{-2}$
10 MBA	18.7 \pm 4.1	9.1 \pm 0.4	0.28	1.4	39	1.18
20 MBA	23.6 \pm 4.6	11.3 \pm 0.6	0.32	1.5	40	1.42
30 MBA	28.8 \pm 5.8	15.8 \pm 0.5	0.24	1.6	38	1.66
50 MBA	52.4 \pm 2.2	40.2 \pm 1.0	0.17	1.9	31	2.28
10 MBA D7	nd	7.0 \pm 0.4	0.29	1.4	48	5.60
20 MBA D7	nd	8.2 \pm 0.6	0.35	1.5	47	5.50
30 MBA D7	nd	15.2 \pm 0.4	0.28	1.6	47	5.36
50 MBA D7	nd	36.0 \pm 0.8	0.19	1.9	nd	5.26

d - nanogel diameter, d_h - nanogel hydrodynamic diameter via volume, Pdl - polydispersity index measured by DLS (SD not higher than 0.03), ρ - density of dry nanogels, $VPTT$ - volume phase transition temperature, Nb - theoretical neutron scattering density, nd - not determined

obtained with good chemical yields and sizes significantly smaller than those previously reported²¹. As determined by DLS (Table 2), the size of nanogels increased with the amount of MBA and was equal to 9 nm for 10% MBA particles and 40 nm for 50% MBA. This trend is the same as that reported for NIPAM MBA cross-linked microgels^{21,35}. All nanogels were approximately circular in appearance as determined by AFM and TEM (see Fig S2 and S3). The cross-section analysis of AFM images was performed and height and width values were determined. Nanogels immobilized on the surface of the substrate exhibited a flattened shape, consistent with previous findings^{36,37}, with average particle height (between 3 and 8 nm) values being much smaller than their diameter (Table 2). The difference in particle size obtained by DLS (in the bulk) and AFM (particles deposited on the support) can be related to the different nature of these characterization techniques, with DLS providing an estimate for the fully solvated hydrodynamic sizes while AFM gives the size of the collapsed nanogels exposed to air. The values of polydispersity index (Pdl) for these systems are also obtained by DLS and are given in Table 2. The data show that higher concentrations of cross-linker result in a less broad size distribution. To gain additional sensitivity to the nanogel structure at the air-water interface for the NR experiments, the corresponding deuterated (NIPAM D7) nanogels were also synthesized and fully characterized prior to the neutron experiments. The H and D nanogels were obtained with similar yields and were found to have similar sizes and morphology. These results suggested that the use of isotopic substitution does not significantly influence polymer structure (Table 2, Fig. S2). Studies of $VPTT$ for all nanogels suggest that the percentage of cross-linker influences the temperature at which the polymer transition occurs (Table 2), as expected given the increase in structure rigidity. At the same time the significant effect on $VPTT$ was observed when changing H in monomer isopropyl group to D.

The data for both H and D nanogels indicate that when the percentage of cross-linker is below or equal to 30%, the characteristics of the materials are comparable. When nanogels are prepared with 50% MBA their properties are significantly different. In particular the size of the nanoparticles is more than double compared to those with lower concentrations of MBA, and the

density of dry polymer is noticeably increased. This suggests that whilst the cross-linker content is high, the rigidity of the polymer network takes a dominant role in determining properties. For these reasons it was decided to focus the interfacial studies only on nanogels with lower amounts of cross-linker (up to 30%), which have much more similar morphologies in the bulk.

Surface behaviour

Adsorption kinetics. The surface pressure (π) deduced from surface tension measurements of NIPAM and NIPAM D7 nanogel dispersions at air/water interface as a function of square root of time is shown in Fig. 1a and 1b. The surface pressure profiles overall are lowered as the percentage of cross-linker increases. This is

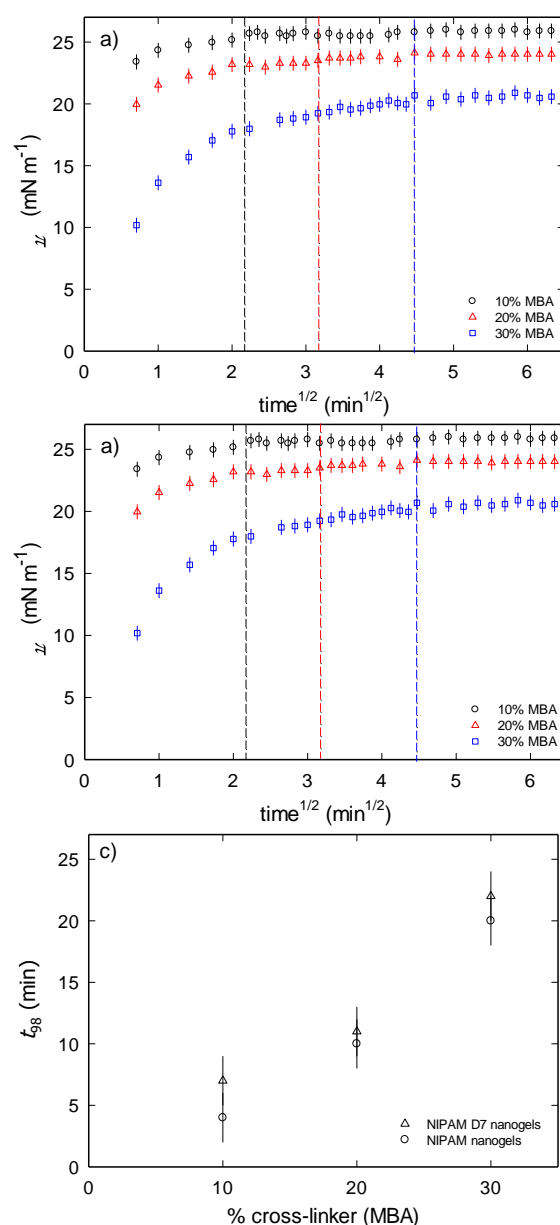


Fig. 1. Adsorption kinetics of NIPAM (a) and NIPAM D7 (b) nanogels at the air/water interface with varying amounts of cross-linker as measured by surface tension (vertical lines refers to t_{98}) and the time taken for the samples to reach equilibrium as a function of cross-linker (c). The bulk nanogel concentration is $5 \times 10^{-3}\text{ mg ml}^{-1}$.

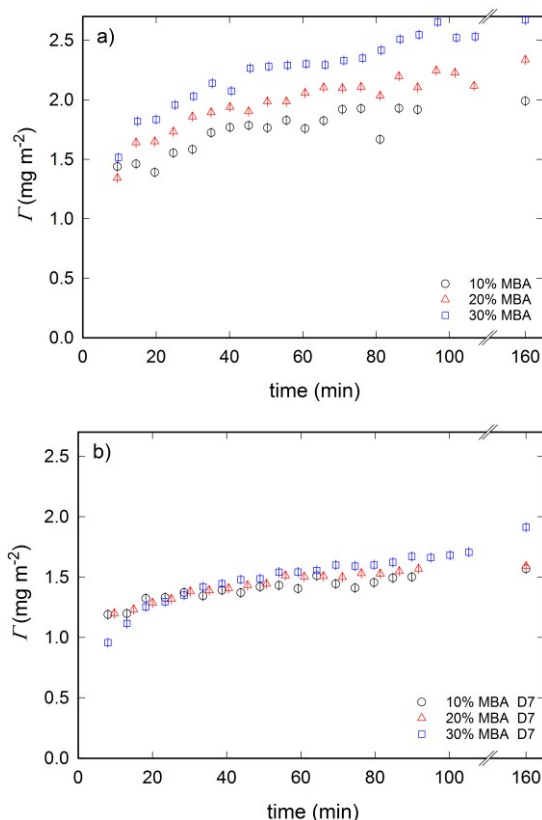


Fig. 2. Adsorption kinetics of NIPAM (a) and NIPAM D7 (b) nanogels at the air/water interface with varying amounts of cross-linker as measured by NR. Values at 160 min correspond to values at equilibrium. The bulk nanogel concentration is $5 \times 10^{-3} \text{ mg ml}^{-1}$.

indicative of a reduction in the surface activity of the nanogels. The rate of equilibration also increases as a function of cross-linker content in nanogels [10% MBA > 20% MBA > 30% MBA]. The time to reach equilibrium (expressed as the time to reach the 98% of final π value, t_{98}) was elongated almost four times when amount of MBA increased from 10 to 30% (Fig. 1c). This observation may be rationalized in terms of the size dependence of the diffusion process. The diffusion coefficients in the bulk can be estimated using the Stokes-Einstein equation; for the 10% MBA (radius of 4.5 nm) $\approx 7.0 \times 10^{-11} \text{ m}^2 \text{ s}^{-1}$ while for 30% MBA (radius of 7.9 nm) $\approx 4.0 \times 10^{-11} \text{ m}^2 \text{ s}^{-1}$. A similar relationship between the adsorption kinetics and amount of incorporated cross-linker was observed by Zhang and Pelton²¹ for NIPAM-based microgels (radius of 270 – 325 nm) cross-linked with MBA, although the reported equilibration times for these microgels were much longer due to their much larger sizes.

The neutron reflectivity profiles as a function of time for the nanogels at the air/NRW interface were measured and the data

were fitted to a single layer model. The fitted parameters were then used to calculate the surface excess (eq. 4) as a function of time (Fig. 2). Both the NR and surface pressure data show that the linear polymers reach adsorption equilibrium at the fastest rate (data not shown). The protonated and deuterated nanogels also show the same trend as surface pressure data – equilibration time is increased with increased amount of cross-linker. However, the equilibration of NIPAM D7 nanogels takes slightly longer than its corresponding protonated ones (compare Γ values at equilibrium). This may be attributed to different bonding energies for H and D, resulting in a different rate of dehydration, as previously suggested³⁸.

The adsorption of nanogels at the air/water interface involves two processes: diffusion of particles towards the interface, followed by a subsequent conformational change of the molecules at the interface. The first stage is size dependent, whilst the second stage is the result of balancing the hydrophobic and hydrophilic moieties (unfolding of polymer chains to optimal configuration) in order to minimize the free energy at the interface. This latter process is driven by the mobility of the individual polymer segments and is influenced by the cross-linker density. Lower degree of cross-linking means the structure can deform (collapse) at the interface more effectively and re-orient the hydrophobic moieties towards the air much faster. These changes are more restricted as the amount of MBA increases and the structure become more rigid (30% MBA nanogels). The two steps of adsorption of NIPAM based microgels were previously reported in the literature^{19–21}. It should be noted that equilibration times deduced from the NR data are much longer than those obtained from the surface pressure measurements. This can be explained in terms of the different sensitivities of these techniques. The surface tension is sensitive primarily to the material present at the interface adjacent to the air due to the change in structure of the surface water; it is only minimally affected by the interactions of particles from the bulk with extended layer morphology due to the high molecular weight of the nanogels. The penetration power of NR allows a much deeper layer away from the interface to be probed. Hence as well as a surface monolayer, material in the underlying adjacent layer will also contribute to the surface excess and thus to the equilibration time. The driving force for this process may be the heterogeneity of nanogels as reported in the literature²¹.

Adsorbed amount. As it was reported before^{16,19}, the adsorption process of nanogels in its initial stage is controlled by the diffusion of particles from the bulk. This is then followed by a much slower reconfiguration of the gels at the interface as described above. Unlike in a surfactant monolayer, the adsorption/desorption dynamics of cross-linked nanogels are slow, so it is not evident if steady state interfacial properties represent true equilibrium. As

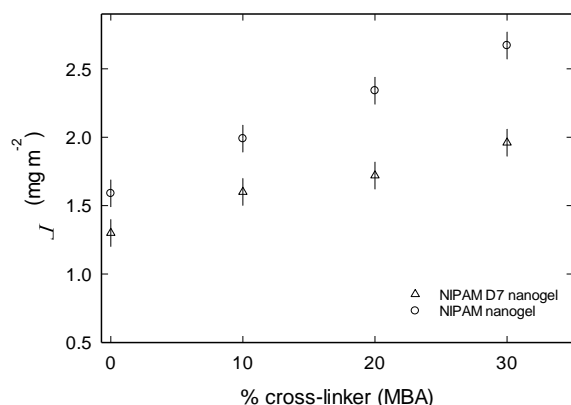


Fig. 3. Surface excess, Γ , of NIPAM (o) and NIPAM D7 (Δ) nanogels with different amount of cross-linker as determined by NR. The bulk nanogel concentration is $5 \times 10^{-3} \text{ mg ml}^{-1}$.

such, the application of Gibbs equation to calculate the adsorbed amount from measurements of the surface tension with respect to the bulk concentration is not valid. Therefore NR is a valuable method for estimating the adsorbed amount.

The NR data for nanogels at the air/NRW interface were first fitted to a simple one-layer model, as described in the experimental section. The fitted parameters for the scattering length density and the layer thickness were then used (eq. 4) to calculate the surface excess (Γ). The surface excess as a function of % of cross-linker is shown in Fig. 3. In order to validate the experimental approach, values of Γ for linear PNIPAM, prepared with both H and D monomers, were measured and found to be around 1.5 mg m^{-2} , which are in close agreement with literature data for protonated NIPAM spread on a Langmuir trough measured by ellipsometry³⁹ and for NIPAM D7 as measured by NR²⁴.

The adsorbed amount of nanogels is greater than that of the linear polymer and depends strongly on MBA content – it increases with amount of cross-linker. As the cross-linker concentration increases, this results in increased hydrophobicity of the nanogel and a higher adsorbed amount. This trend is the same for both the H and D nanogels; however, there is a considerable difference between the adsorbed amounts of the two polymers, which increases with the percentage of cross-linker. The protonated nanogels showing higher values compared to the deuterated counterparts (with $\Gamma = 2.67 \text{ mg/m}^2$ for 30% MBA and 1.96 mg/m^2 for 30% MBA D7). It is important to note that the surface excess is a function of temperature and all measurements in this paper were carried out

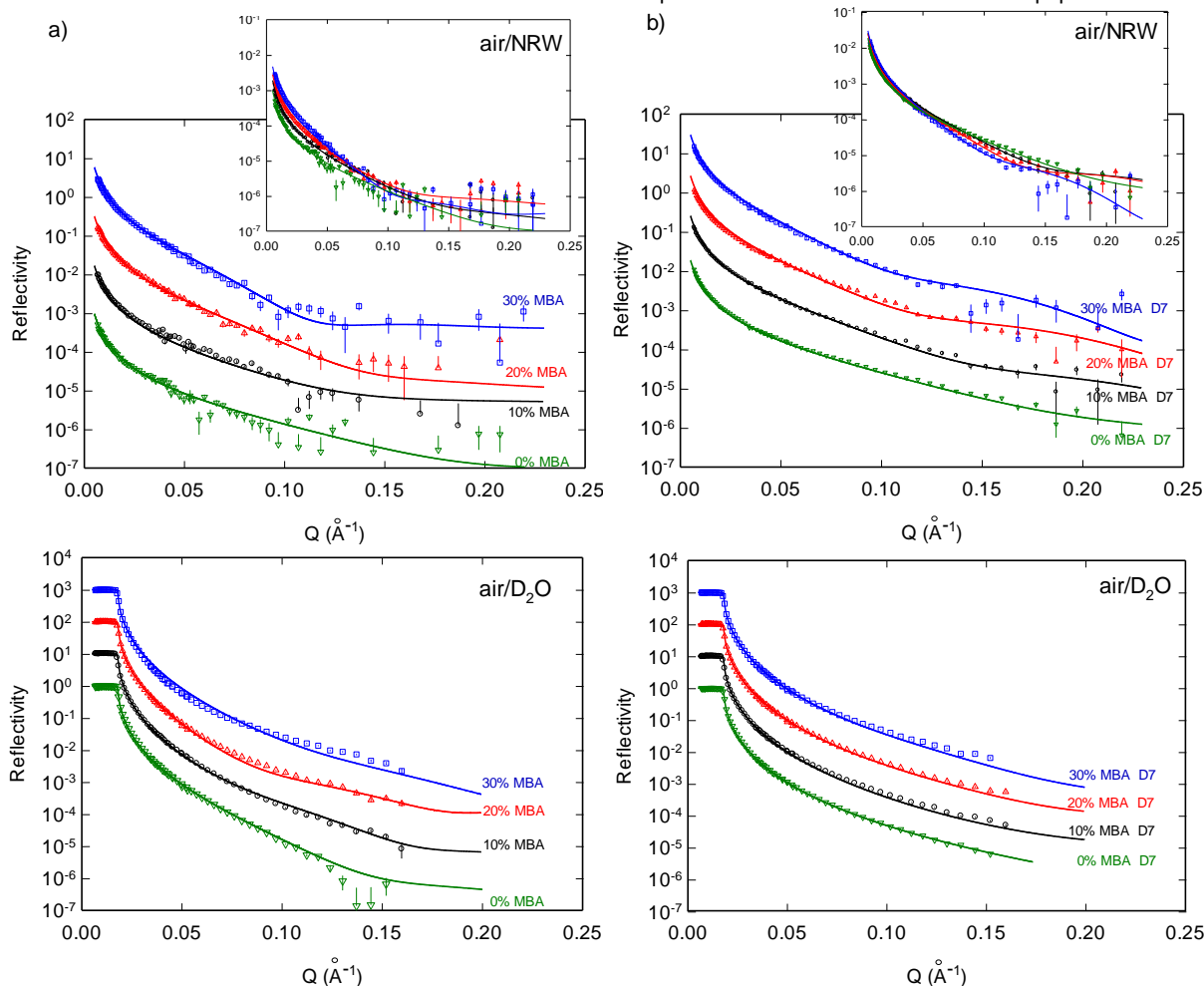


Fig. 4. Neutron reflectivity profiles of NIPAM (a) and NIPAM D7 (b) nanogels at the air/NRW (upper panel) and air/D₂O (lower panel) interfaces. The bulk nanogel concentration is $5 \times 10^{-3} \text{ mg ml}^{-1}$. The solid lines are fits to the data. The profiles are shifted by factors of 10 for the purpose of clarity and the insets show the data not shifted.

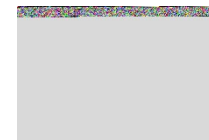


Table 3. Summary of model fits of NR data of NIPAM and NIPAM D7 nanogels at the air/water interface

sample	air/null reflecting water			air/D ₂ O		
	<i>d</i> (Å)	<i>Nb</i> _{fitted} (10 ⁻⁶ Å ⁻²)	<i>σ</i> (Å)	<i>d</i> (Å)	<i>Nb</i> _{fitted} (10 ⁻⁶ Å ⁻²)	<i>σ</i> (Å)
0 MBA	7	0.99	4	7	1.86	4
	20	0.27	10	20	5.65	10
	-	-	-	-	-	-
10 MBA	14	0.75	4	14	2.05	4
	10	0.37	5	10	6.19	6
	15	0.17	3	15	5.62	3
20 MBA	14	0.88	5	14	2.50	5
	18	0.42	6	18	6.26	6
	13	0.20	3	13	5.65	3
30 MBA	17	0.94	8	17	3.09	8
	26	0.49	7	26	6.31	7
	10	0.24	5	10	5.69	5
0 MBA D7	7	5.79	4	7	5.63	4
	20	0.72	10	20	6.32	10
	-	-	-	-	-	-
10 MBA D7	14	3.55	4	14	4.74	4
	10	0.49	5	10	6.29	6
	15	0.79	3	15	6.24	3
20 MBA D7	14	3.41	5	14	5.03	5
	18	0.44	6	18	6.28	6
	13	0.78	3	13	6.23	3
30 MBA D7	17	3.04	8	17	5.19	5
	26	0.45	7	26	6.23	7
	10	0.76	5	10	6.21	5

d – layer thickness ± 1 Å, *Nb*_{fitted} – fitted scattering length density, *σ* – roughness

at a physiological temperature of 309 K. However, the VPTT values are different for the H and the D nanogels, hence the deviation in the measured values of Γ . This is discussed later in the context of isotope effects resulting in different bonding energies.

Nanogel structure at the interface. The neutron reflectivity profiles for both H and D nanogels with different % of cross-linkers were measured at the air/NRW and air/D₂O interfaces to ascertain detailed structural information about the nanogels, Fig. 4. Although PNIPAM, a linear polymer, is a very different type of material from the cross-linked nanogels, it was included in this analysis to validate the applied approach. A two-layer model was required to fit the data for the linear polymer while the nanogels (with cross-linker) required a minimum of a three-layer model to fit consistently all four isotopic contrasts. The inadequacy of one layer model representation of the data is shown in the supporting information (Fig. S4). The best fit for each set of data is shown on the graph by a solid line (Fig. 4) while the resulting parameters are given in Table 3. The scattering length density profiles for these fits were then used

to estimate the volume fraction profiles of the nanogels at the interface, Fig. 5. The volume fraction profiles for the linear polymer show two distinct regions. The first region consists of a densely packed layer in contact with air; which has collapsed polymer chains and low water content (less than 10%; thickness of 7 Å). The second more diffuse regions consist of highly solvated polymer (88% water) extending towards the bulk water. A similar conformation for linear PNIPAM at the air/water interface has been reported previously²⁵. The reflectivity data for the nanogels were fitted using a three-layer model. The fitted parameters are given in Table 3. Again the first layer consists of a condensed (collapsed) layer of polymer. The thickness of this layer increases with the % of cross-linker. The first layer is then followed by gradually diffusing second and third layers. In the first layer the value of $\phi_{polymer}$ was equal to 0.64, 0.62 and 0.57 for nanogels with 10, 20 and 30% of MBA, respectively (and was the same for both the H and D gels). This region was characterized by low water content similar to that reported for a collapsed microgel at temperatures above VPTT²⁴. The content of water in this layer varies monotonically with MBA

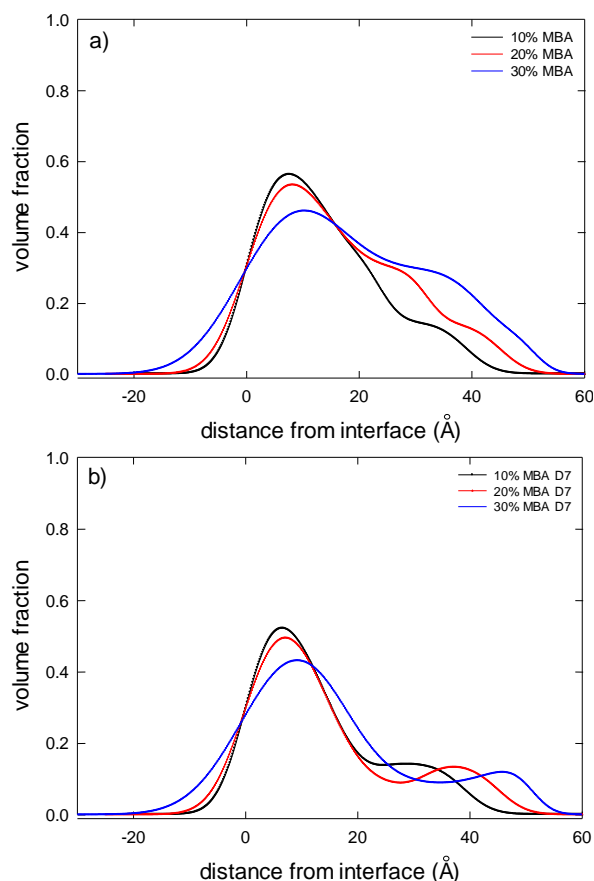


Fig. 5. Volume fraction of a) NIPAM and b) NIPAM D7 nanogels at the air/water interface calculated based on the neutron reflectivity profiles.

concentration, $\varphi_{water} = 0.18, 0.26$ and 0.34 for 10, 20 and 30% MBA, respectively. This can be attributed to a reduction in the nanogel ability to change conformation (and thus repel water from polymer network) of the gels with a higher degree of cross-linking. The second layer consists of fully solvated polymer with a low volume fraction. The volume fractions for H and D nanogels are different, 0.08 for D and 0.30 for H nanogels. This is attributed to different VPTT values for H and D nanogels. We relate this observation to isotope effects resulting in different bonding energies (especially ability to create hydrogen bonds) for the protonated and deuterated isopropyl groups. The influence of

isotopes on physical properties of polymers has been reported already in literature⁴⁰.

The volume fraction profiles of the second layer for D nanogels (where only the isopropyl group of the NIPAM is deuterated) show a low scattering length density region, which suggests it consist mainly of MBA. The thickness of this layer increases with the increase of cross-linker concentration ($d = 10, 18$ and 26 \AA for gels with 10, 20 and 30% of MBA, respectively) as expected.

The fitting of the data is very sensitive to the presence of a third layer. In the case of NIPAM D7 particles Nb_{fitted} has values higher than for the second layer suggests a region rich in deuterated moieties. Low $\varphi_{polymer}$ for NIPAM gels indicates lower polymer density. For both H and D particles this means the presence of pending PNIPAM chains that are very loosely cross-linked forming a shell-like structure with thickness of between 10-15 \AA , which is thinner for nanogels with a higher concentration of MBA. This interpretation of the data is further supported by similar findings for NIPAM based microgels (with particle size $\sim 200 \text{ nm}$) where the difference in polymerization rates between the monomer and cross-linker plays a key role^{35,41}. As a result, the structure of the gel particles depends strongly on the degree of cross-linking. At high cross-linker concentrations, particles are described with a Gaussian segment density distribution (i.e. a highly cross-linked core). With decreasing cross-linking density the structure of the gel particles changes toward that of a highly branched coil³⁵.

Given the diffuse nature of the interface, we then allowed the values of the layer roughness to vary in the fitting procedure. It was found that the layer roughness increased slightly with increasing amount of cross-linker (Table 3). This can be attributed to the rigidity/elasticity of the nanogels, which increases with increasing concentration of MBA. Matzelle *et al.* have studied the elastic properties of NIPAM hydrogels cross-linked with MBA (up to 5 mol %) by scanning force microscopy⁴². They found that Young's moduli of the gels were strongly dependent on the amount of MBA and increased by almost factor of 4 when the % of MBA was increased from 1 to 5%. This suggests that the nanogels with 30% of cross-linker may adopt an even less flexible structure, hence an increase in the interfacial roughness is physically reasonable.

The structural conformations of the nanogels as a function of the % of cross-linker are shown schematically in Fig. 6, reflecting the

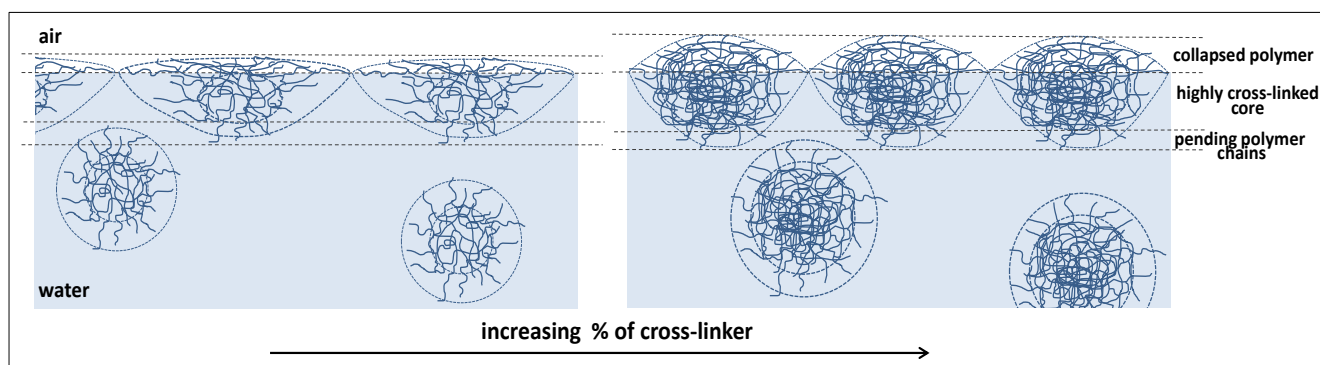


Fig. 6. Schematic representation of nanogels structure, with different degree of cross-linking at the air/water interface.

differences in the physical structures measured while taking into account their associated degree of flexibility. A higher flexibility of the gels means a higher surface coverage will result at lower adsorbed amounts. Comparable behaviour of NIPAM-based microgels on the solid substrate was observed and reported before⁴³. The structural conformations are also reflected in the adsorbed layer thickness determined using NR. These values are approximately half the size of the nanogel observed by DLS in the bulk, providing additional evidence for the collapsed nature of the nanogels at the air-water interface. Similar behaviour was observed recently in mixtures of poly(amido amine) dendrimers with the surfactant sodium dodecyl sulfate⁴⁴, where the ability of the dendrimer to deform at the interface was related to its size and flexibility. Such a behaviour of NIPAM based microgels liquid/liquid interfaces was suggested before^{12,19,45} although no direct experimental evidence was provided.

Conclusions

In this study we have characterized the behaviour of *N*-isopropylacrylamide-based nanogels cross-linked with *N,N'*-methylenebisacrylamide at the air/water interface, demonstrating that the degree of cross-linking has a profound effect on their adsorption kinetics, adsorbed amount and structures created. Like conventional short-chain surfactants, NIPAM nanogels lower the surface tension of water; however, because of the lack of well-defined hydrophobic and hydrophilic regions (i.e. a head and tail) they form more complex structures at the interface, which have to date not been resolved. As shown by neutron reflectivity measurements, the structure of the adsorbed material can be represented by three distinct regions: a densely packed polymer with low water content in contact with air, followed by a fully solvated, highly cross-linked region, and finally a region of polymer chains that extend towards the bulk solution.

The structural data also suggest an extensive rearrangement of the conformation of the nanogel particles at the interface during the adsorption process, resulting in structural deformation. The degree of deformation diminishes with increasing % of cross-linker. It is interesting to note that although differences in conformations between the bulk and the liquid/liquid interface for NIPAM-based microgels have been previously hypothesized, this was never demonstrated. In this paper we provide experimental evidence that such behaviour indeed occurs for NIPAM-based nanogels at the air/water interface.

The data presented are an important input into understanding the behaviour of gel particles at interfaces. We believe that they may lead to achievement of the rational, smart design of novel materials for specific applications.

Acknowledgements

We thank the ILL for beam time on FIGARO and Simon Wood for technical assistance during the experiment. The European Commission (FP7 Marie Curie Actions, NANOLEM, PIEF-GA-

2013-627146 to KZ) and the Chinese Scholarship Council (studentship to HS) are gratefully acknowledged for financial support.

References

- 1 R. Paull, J. Wolfe, P. Hebert, M. Sinkula, *Nature Biotechnol.*, 2003, **21**, 1134–1147.
- 2 O. V. Salata, *J. Nanobiotechnology*, 2004, **2**, 3–9.
- 3 J. P. Rao, K. E. Geckeler, *Prog. Polym. Sci.*, 2011, **36**, 887–913.
- 4 C. Vauthier, K. Bouchemal, *Pharm. Res.*, 2009, **26**, 1025–1058.
- 5 S. C. Maddock, P. Pasetto, M. Resmini, *Chem. Comm.*, 2004, **5**, 536–537.
- 6 J. K. Oh, R. Drumright, D. J. Siegwart, K. Matyjaszewski, *Prog. Polym. Sci.*, 2008, **33**, 448–477.
- 7 R. Pelton, *Adv. Colloid Interf. Sci.*, 2000, **85**, 1–33.
- 8 K. Park, H. Park, Smart Hydrogels, in: J.C. Salamone (Ed.), *Concise Polymeric Materials Encyclopedia*, CRC Press, Boca Raton, 1999, pp. 1476–1478.
- 9 B. R. Saunders, N. Laajam, E. Daly, S. Teow, X. Hu, R. Stepto, *Adv. Colloid Interf. Sci.*, 2009, **147–148**, 251–262.
- 10 A. Cameron, *Nature Mater.*, 2008, **7**, 767–768.
- 11 Y. Guan, Y. Zhang, *Soft Matter*, 2011, **7**, 6375–6384.
- 12 Z. Li, T. Ngai, *Nanoscale*, 2013, **5**, 1399–1410.
- 13 V. Carias, J. Wang, R. Toome, *Langmuir*, 2014, **30**, 4105–4110.
- 14 B. Brugger, B. A. Rosen, W. Richtering, *Langmuir*, 2008, **24**, 12202–12208.
- 15 M. Destribats, V. Lapeyre, E. Sellier, F. Leal-Calderon, V. Schmitt, V. Ravaine, *Langmuir*, 2011, **27**, 14096–14107.
- 16 O. S. Deshmukh, D. van den Ende, M. Cohen Stuart, F. Mugele, M. H. G. Duits, *Adv. Colloid Interf. Sci.*, 2014, **222**, 215–227.
- 17 W. Richtering, *Langmuir*, 2012, **28**, 17218–17229.
- 18 J. Zhang, R. Pelton, *Langmuir*, 1996, **12**, 2611–2612.
- 19 O. S. Deshmukh, A. Maestro, M. H. G. Duits, D. van den Ende, M. Cohen Stuart, F. Mugele, *Soft Matter*, 2014, **10**, 7045–7050.
- 20 J. Zhang, R. Pelton, *Colloids Surf. A*, 1999, **156**, 111–122.
- 21 J. Zhang, R. Pelton, *Langmuir*, 1999, **15**, 8032–8036.
- 22 Y. Cohin, M. Fisson, K. Jourde, G. G. Fuller, N. Sanson, L. Talini, C. Monteux, *Rheol. Acta*, 2013, **52**, 445–454.
- 23 J. Reguera, E. Ponomarev, T. Geue, F. Stellacci, F. Bresme, M. Moglianetti, *Nanoscale*, 2015, **7**, 5665–5673.
- 24 R. M. Richardson, R. Pelton, T. Cosgrove, J. Zhang, *Macromolecules*, 2000, **33**, 6269–6274.
- 25 L. T. Lee, B. Jean, A. Menelle, *Langmuir*, 1999, **15**, 3267–3272.
- 26 P. Çakir, A. Cutivet, M. Resmini, B.T.S. Bui, K. Haupt, *Adv. Mater.*, 2013, **25**, 1048–1051.
- 27 A. Servant, S. Rogers, A. Zorbakhsh, M. Resmini, *New J. Chem.*, 2013, **37**, 4103–4109.
- 28 R. A. Campbell, H. P. Wacklin, I. Sutton, R. Cubitt, G. Fragneto, *Eur. Phys. J. Plus*, 2011, **126**, 107.
- 29 J. R. Lu, Z. X. Li, R. K. Thomas, J. Penfold, *J. Chem. Soc., Faraday Trans.*, 1996, **92**, 403–408.
- 30 Heavens, O. S. In *Optical Properties of Thin Films*; Butterworth: London, 1955.
- 31 A. Angus-Smyth, R. A. Campbell, C. D. Bain, *Langmuir*, 2012, **28**, 12479–12492.
- 32 Á. Abraham, R. A. Campbell, I. Varga, *Langmuir*, 2013, **29**, 11554–11559.
- 33 J. R. Lu, R. K. Thomas, J. Penfold, *Adv. Colloid Interf. Sci.*, 2000, **84**, 143–304.
- 34 A. Nelson, *J. Appl. Cryst.*, 2006, **39**, 273–276.
- 35 I. Varga, T. Gilányi, R. Mészáros, G. Filipcsei, M. Zrínyi, *J. Phys. Chem. B*, 2001, **105**, 9071–9076.
- 36 X. Hu, Z. Tong, L. A. Lyon, *Langmuir*, 2011, **27**, 4142–4148.
- 37 O. Tagit, N. Tomczak, G. J. Vancso, *Small*, 2008, **4**, 119–126.
- 38 H. Shirota, K. Horie, *Chem. Phys.*, 1999, **242**, 115–121.

ARTICLE

Journal Name

- 39 M. Kawaguchi, W. Saito, T. Kato, *Macromolecules*, 1994, **27**, 5882–5884.
- 40 H. Shirota, N. Endo, K. Horie, *Chemical Physics*, 1998, **238**, 487–494.
- 41 B. Sierra-Martin, J. R. Retama, M. Laurenti, A. Fernández Barbero, E. López Cabarcos, *Adv. Colloid Interf. Sci.*, 2014, **205**, 113–123.
- 42 T. R. Matzelle, G. Geuskens, N. Kruse, *Macromolecules*, 2003, **36**, 2926–2931.
- 43 O. Tagit, N. Tomczak, G. J. Vancso, *Small*, 2008, **4**, 119–126.
- 44 M. Yanez Arteta, R. A. Campbell, T. Nylander, *Langmuir*, 2014, **30**, 5817–5828.
- 45 B. R. Saunders, *Langmuir*, 2004, **20**, 3925–3932.

Smart nanogels at the air/water interface: structural studies by neutron reflectivity

Katarzyna Zielińska,^a Huihui Sun,^a Richard A. Campbell,^b Ali Zorbakhsh^{a*} and Marina Resmini^{a*}

^a Department of Chemistry, SBCS, Queen Mary, University of London, Mile End Road, London E1 4NS, United Kingdom, e-mails: a.zorbakhsh@qmul.ac.uk, m.resmini@qmul.ac.uk

^b Institut Laue-Langevin, 71 avenue des Martyrs - CS 20156, 38042 Grenoble Cedex 9, France

Supporting information

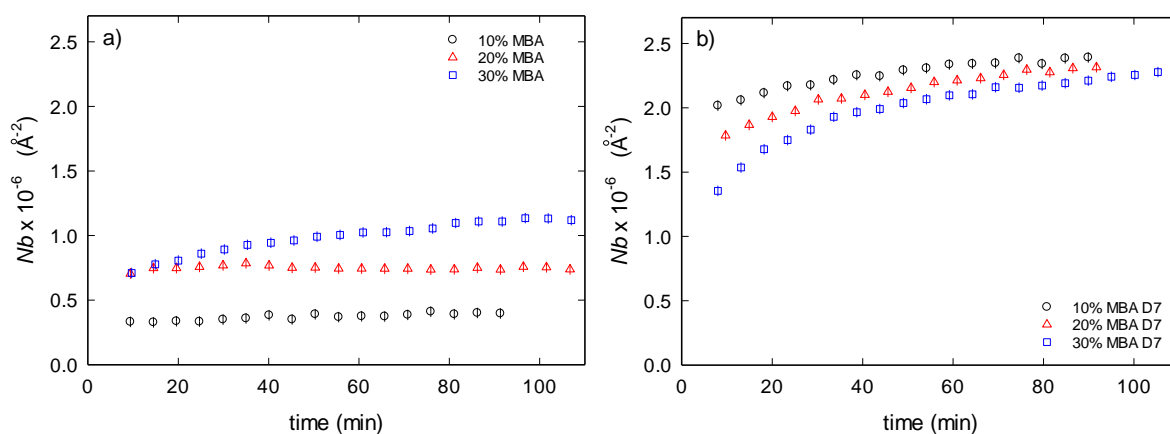


Fig. S1. Scattering length density (Nb) as a function of time for NIPAM (a) and NIPAM D7 (b) nanogels with varying amounts of cross-linker at the air/NRW interface. The bulk nanogel concentration is $5 \times 10^{-3} \text{ mg ml}^{-1}$.

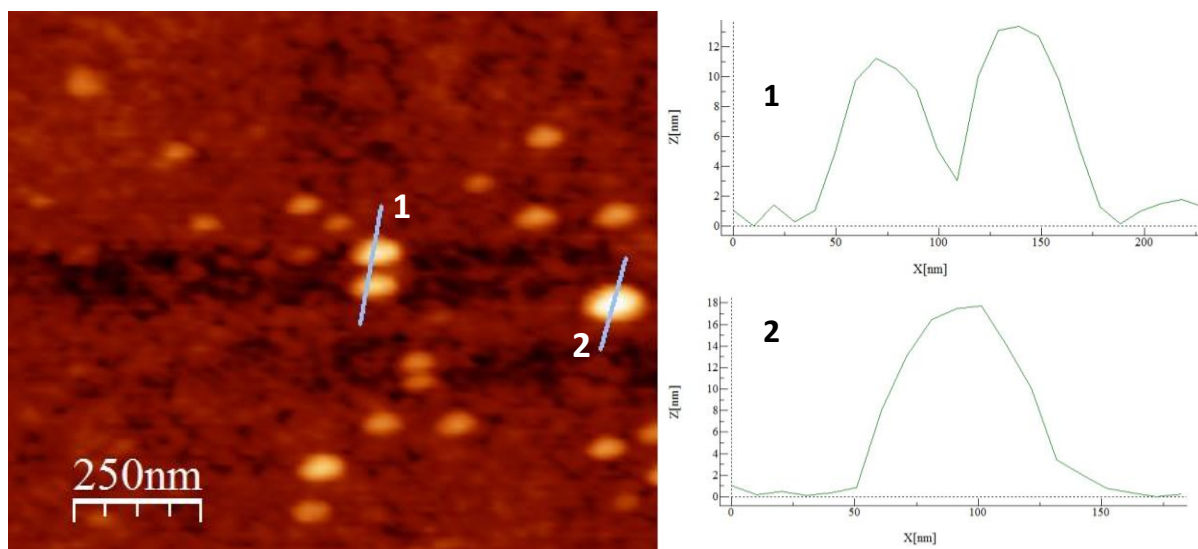


Fig. S2. AFM image and cross-section of NIPAM nanogels containing 30% of MBA.

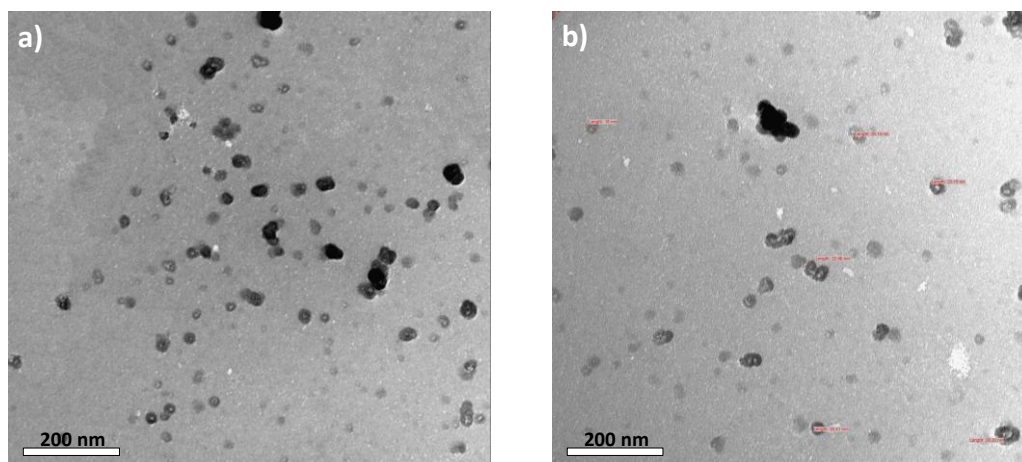


Fig. S3. TEM images of NIPAM (a) and NIPAM D7 (b) nanogels containing 20% of MBA.

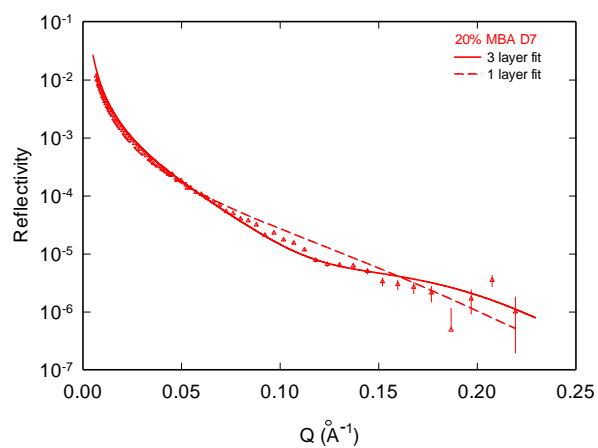


Fig. S4. Neutron reflectivity profiles of NIPAM D7 nanogels with 20% of MBA at the air/NRW interfaces. The bulk nanogel concentration is $5 \times 10^{-3} \text{ mg ml}^{-1}$. The solid and dashed lines represent the one and three layer fits to the data, respectively.